# A Self-Assembling and Disassembling (SADA) Bispecific Antibody (BsAb) Platform for Curative Two-step Pretargeted Radioimmunotherapy

Brian H. Santich[1], Sarah M. Cheal[2], Mahiuddin Ahmed[1], Michael R. McDevitt[2,3,4], Ouathek Ouerfelli[5], Guangbin Yang[5], Darren R. Veach[2], Edward K. Fung[3], Mitesh Patel[2], Daniela Burnes Vargas[2], Aiza A. Malik[1], Hong-Fen Guo[1], Pat B. Zanzonico[6], Sebastien Monette[7], Adam O. Michel[7], Charles M. Rudin[2], Steven M. Larson[2,3], and Nai K. Cheung[1]

## ABSTRACT

**Purpose:** Many cancer treatments suffer from dose-limiting toxicities to vital organs due to poor therapeutic indices. To overcome these challenges we developed a novel multimerization platform that rapidly removes tumor-targeting proteins from the blood to substantially improve therapeutic index.

**Experimental Design:** The platform was designed as a fusion of a self-assembling and disassembling (SADA) domain to a tandem single-chain bispecific antibody (BsAb, anti-ganglioside GD2 × anti-DOTA). SADA–BsAbs were assessed with multiple *in vivo* tumor models using two-step pretargeted radioimmunotherapy (PRIT) to evaluate tumor uptake, dosimetry, and antitumor responses.

**Results:** SADA–BsAbs self-assembled into stable tetramers (220 kDa), but could also disassemble into dimers or monomers (55 kDa) that rapidly cleared via renal filtration and substantially reduced immunogenicity in mice. When used with rapidly clearing DOTA-caged PET isotopes, SADA–BsAbs demonstrated accurate tumor localization, dosimetry, and improved imaging contrast by PET/CT. When combined with therapeutic isotopes, two-step SADA-PRIT safely delivered massive doses of alpha-emitting ($^{225}$Ac, 1.48 MBq/kg) or beta-emitting ($^{177}$Lu, 6,660 MBq/kg) S-2-(4-aminobenzyl)-1,4,7,10-tetraazacyclododecane tetraacetic acid (DOTA) payloads to tumors, ablating them without any short-term or long-term toxicities to the bone marrow, kidneys, or liver.

**Conclusions:** The SADA–BsAb platform safely delivered large doses of radioisotopes to tumors and demonstrated no toxicities to the bone marrow, kidneys, or liver. Because of its modularity, SADA–BsAbs can be easily adapted to most tumor antigens, tumor types, or drug delivery approaches to improve therapeutic index and maximize the delivered dose.

*See related commentary by Capala and Kunos, p. 377*

## Introduction

Metastatic disease remains a major challenge to cancer cures (1). While localized disease can be controlled by surgery or radiotherapy, widespread, distant, and occult metastases require systemic therapies (2). However, many of these treatments have unintended dose-limiting toxicities to vital organs due to poor therapeutic indices (the ratio of total drug uptake in the tumor compared with other normal tissues; ref. 3), which results in many patients receiving subtherapeutic doses of treatment followed invariably by tumor relapse. Even with tumor-specific targets, conventional one-step delivery systems typically have therapeutic index below 10:1 (4).

Multi-step targeting strategies (5), where tumor-targeting agents (e.g., antitumor IgG) are delivered separately from the cytotoxic payloads (e.g., chelated radioisotopes), have improved therapeutic indices, but dose-limiting toxicities remain. In conventional two-step pretargeted radioimmunotherapy (PRIT), the use of long-lived IgG molecules often results in myelotoxicity due to unbound IgG capturing and circulating the radioisotope (**Fig. 1A**; ref. 6). Although specially designed clearing agents can be used to remove this IgG, the resulting three-step PRIT becomes substantially more complicated to translate to the clinic because the optimal clearing agent dose must be carefully titrated to individual tumor size and antigen density (7): administering too little risks insufficiently clearing the IgG, while administering too much risks interfering with payload uptake at the tumor (8). To safely maximize the administered dose in a clinically feasible way, the delivery strategy must use a two-step approach (no clearing agent) with a tumor-targeting platform that can clear itself from the blood, bone marrow, liver, kidneys, and other tissues.

In this study, we engineered such a platform using specially designed self-assembling and disassembling (SADA) domains (**Fig. 1B**). When fused to bispecific antibodies (BsAb), the resulting SADA–BsAbs self-assembled into stable tetrameric complexes (220 kDa) that bound tumors with high avidity, but could also disassemble into small dimers (110 kDa) or monomers (55 kDa) after a period of circulation in the blood (hours). Importantly, while the tetrameric complex exceeded the molecular weight cutoff for renal filtration, the small monomers fell below the threshold (∼<70 kDa) and were rapidly and completely cleared from the blood. When combined with alpha- or beta-emitting radioisotopes, two-step SADA-PRIT delivered massive doses of radiation ($^{225}$Ac 1.48 MBq/kg and $^{177}$Lu 6,660 MBq/kg) to established solid tumors in multiple mouse models and ablated them without any

[1]Department of Pediatrics, Memorial Sloan Kettering Cancer Center, New York, New York. [2]Molecular Pharmacology Program, Memorial Sloan Kettering Cancer Center, New York, New York. [3]Department of Radiology, Weill Cornell Medical College, New York, New York. [4]Department of Radiology, Memorial Sloan Kettering Cancer Center, New York, New York. [5]Organic Synthesis Core Facility, Memorial Sloan Kettering Cancer Center, New York, New York. [6]Department of Medical Physics, Memorial Sloan Kettering Cancer Center, New York, New York. [7]Laboratory of Comparative Pathology, Memorial Sloan Kettering Cancer Center, The Rockefeller University, Weill Cornell Medicine, New York, New York.

**Note:** Supplementary data for this article are available at Clinical Cancer Research Online (http://clincancerres.aacrjournals.org/).

**Corresponding Author:** Nai K. Cheung, Memorial Sloan Kettering Cancer Center, 1275 York Avenue, Box 170, Z-1403, New York, NY 10065. Phone: 1646-888-2313; Fax: 646-422-0452; E-mail: cheungn@mskcc.org

Clin Cancer Res 2021;27:532–41

**doi:** 10.1158/1078-0432.CCR-20-2150

## Translational Relevance

More than 90% of cancer therapeutics currently in clinical development will fail, mostly due to dose-limiting toxicities or subtherapeutic recommended phase II dose levels, a consequence of insufficient therapeutic index. We have developed a novel drug delivery platform [self-assembling and disassembling (SADA)] with unique pharmacokinetics that allowed for dramatic improvements in therapeutic index and substantially reduced immunogenicity. As a diagnostic tool, SADA visualized tumors with high precision using PET. As a therapeutic, SADA durably ablated two aggressive solid tumors (small-cell lung cancer and neuroblastoma) using $^{177}$Lu or $^{225}$Ac, without any toxicity to the bone marrow, liver, or kidney. To the best of our knowledge, this is the first example of a curative radioimmunotherapy strategy without such toxicities. Furthermore, SADA is highly modular and can be adapted to improve many other drug delivery systems. On the basis of the findings presented here, the SADA platform has entered development for first-in-human clinical trials.

clinical or histologic toxicities to the bone marrow, liver, kidneys, spleen, or brain.

## Materials and Methods

### Protein expression, reagents, and binding studies

SADA proteins were expressed using the Expi293 Expression System (Invitrogen) and purified by Affinity Chromatography (GE Healthcare, Ni-NTA Gravitrap, catalog no., 11003399). S-2-(4-Aminobenzyl)-1,4,7,10-tetraazacyclododecane tetraacetic acid (DOTA, ~580 g/mol) was purchased from Macrocyclics and DOTA[$^{175}$Lu]-thiourea-PEG$_4$-1,4,7,10-tetraazacyclododecane-1,4,7-triyl)triacetic acid[metal] (Proteus, ~1,350 g/mol) was synthesized at Memorial Sloan Kettering Cancer Center (New York, NY) according to previously described methods (9). Surface plasmon resonance (GE Healthcare, Biacore T200) was performed as described previously (10).

### Radiometal labeling

DOTA was labeled with $^{86}$Y nitrate (Radiological Chemistry and Imaging Laboratory at Washington University in St. Louis, St. Louis, MO) or $^{177}$LuCl$_3$ (PerkinElmer) using previously described methods (2). Proteus was labeled with $^{225}$Ac nitrate (Oak Ridge National Laboratory) as described previously (9). Radioisotopes were given 48 hours after P53-SADA-BsAb in every study.

### Animal studies

Greater detail on radiolabeling, pharmacokinetic studies, and histologic analyses are provided in the Supplementary Data. All animal experiments were performed in compliance with an Institutional Animal Care and Use Committee–approved protocol (protocols 09-05-010 and 86-02-020). Unless otherwise stated, BsAb doses were administered retro-orbitally and all tumors were implanted subcutaneously in the right flank of the mice. Weights and tumor volumes were measured once per week, and overall mouse health was evaluated at least three times per week. Mice were sacrificed once tumor volumes reached 1,500–2,000 mm$^3$. Animal experiments used either C57BL/6J (Jackson Laboratories, catalog no., 000664), athymic nude (Envigo), NOD Prkdc$^{scid}$ IL2rgc$^{-/-}$ (NSG, Jackson Laboratories, catalog no., 005557), or *Balb/c Rag2*$^{-/-}$ *IL2rgc*$^{-/-}$ mice (BRG, Taconic, catalog no., 11503). All mice from the same treatment groups were cohoused in the same cage. Experiments using female mice were completely randomized before their initial treatment. Experiments using male mice had cages randomized before the start of treatment. Blinding of treatment or experimental measurements was not carried out.

### Cell lines and tumor models

*In vitro* experiments were performed on a luciferase-transfected IMR32 neuroblastoma cell line. *In vivo* studies used either IMR32

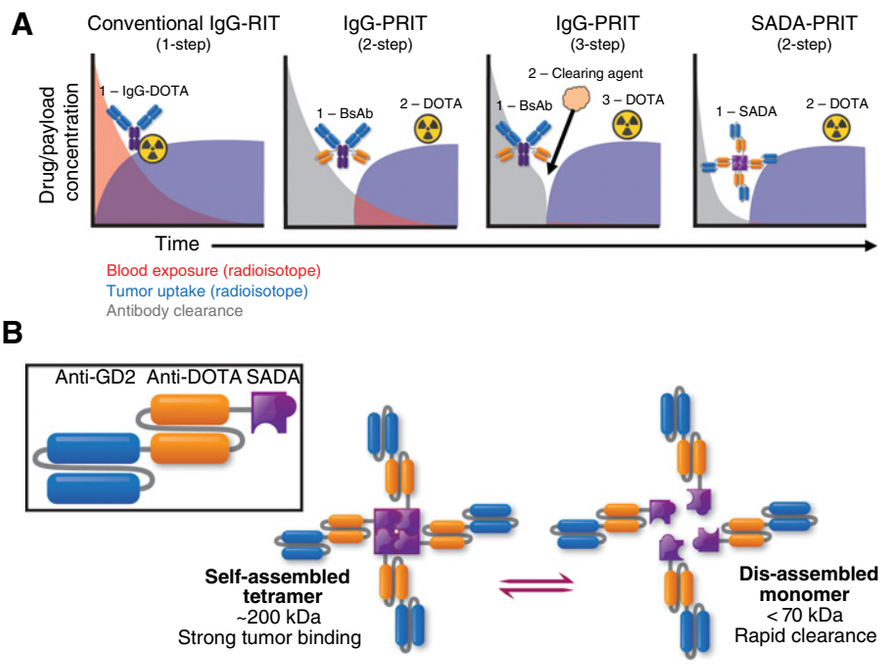


**Figure 1.**
Overview of multi-step radioimmunotherapy. **A,** Schematic of four different radioimmunotherapy (RIT) strategies. Representative antibodies, radioisotope payloads, and clearing agents are included for reference. Blue antibody domains are tumor specific, and orange domains are DOTA specific. The red curve represents concentration of radioisotope in the blood over time, blue represents the concentration of radioisotope in the tumor, and gray represents the concentration of nonradioactive antibody in the blood. **B,** Representative P53-SADA-BsAb. Each monomer (inset) is made of three domains: an antitumor domain (blue), an anti-DOTA domain (orange), and a SADA domain (purple), from N-terminus to C-terminus, respectively. SADA domains self-assemble into tetramers (~200 kDa), but also disassemble into monomers (~50 kDa).

(ATCC, CCL-127) or patient-derived xenograft (PDX) tumors obtained from neuroblastoma or small-cell lung cancer (SCLC) surgical specimens.

### Pharmacokinetics analysis

Serum concentrations of BsAbs were determined by ELISA as described previously (11). Pharmacokinetics analysis was carried out by noncompartmental analysis of the serum concentration–time data using WinNonlin software program (Pharsight Corp.).

### PET/CT imaging analysis

Female nude mice [Hsd:athymic Nude-*Foxn1*$^{nu}$ 069(nu)/070 (nu/+)] were implanted with IMR32 neuroblastoma tumors on day 0 and treated with BsAb and DOTA[$^{86}$Y] (3.7 MBq, 30 pmol) on days 16 and 18, respectively. Mice treated with three-step IgG-scFv-BsAb (8) received 25 μg of a DOTA-dendrimer clearing agent (7) 4 hours prior to the administration of DOTA[$^{86}$Y]. Mice were imaged using PET/CT (Siemens, Inveon PET/CT) 16 hours later, with PET data collected for 30 minutes (a minimum of $1 \times 10^6$ coincidence events) followed whole-body CT scans acquired with a voltage of 80 kV and 500 μA. Image data were normalized to correct for nonuniformity of response of the PET, dead-time count losses, positron branching ratio, and physical decay to the time of injection, but no attenuation, scatter, or partial volume averaging correction was applied.

### Tissue biodistribution analysis and dosimetry

Female nude mice were implanted with IMR32 tumors on day 0 in their right flank. Established tumors were treated with BsAb on day 16 and with DOTA[$^{177}$Lu] (1.85–18.5 MBq) on day 18. At 2, 24, 48, or 120 hours after administration of DOTA[$^{177}$Lu], tissues were excised for Gamma Scintillation Counting (PerkinElmer). Dosimetry estimates were modeled using the nondecay-corrected time–activity concentration data fit to a one-component, two-component, or more complex exponential function as appropriate, and analytically integrated to yield the accumulated activity concentration per administered activity (MBq-hour/g per MBq). The $^{177}$Lu equilibrium dose constant for nonpenetrating radiations (8.49 g-cGy/MBq-hour) was used to estimate the tumor-to-tumor and select organ-to-organ self-absorbed doses, assuming complete local absorption of the $^{177}$Lu beta rays only and ignoring the gamma rays and nonself-dose contributions.

### Immunogenicity analysis

C57BL/6J mice were injected with P53-SADA-BsAb or IgG-scFv-BsAb (0.5 nmol) on days 0 and 28, intravenously and intraperitoneally, respectively. Plasma were obtained on days 27 and 55. Antidrug antibody (ADA) concentrations were determined by ELISA. Wells were coated with the corresponding BsAbs, blocked with BSA (0.5% in PBS), and incubated with plasma samples in duplicates. Binding was detected using an horseradish peroxidase–conjugated goat anti-mouse antibody (Jackson ImmunoResearch) and developed with o-phenylenediamine (Sigma). For quantitation, standard curves were generated using either mouse-anti-HIS (P53-SADA-BsAb) or mouse-anti-human IgG-hinge (IgG-scFv-BsAb) antibodies. Absorbance was measured at 490 nm (Synergy) and concentrations were estimated using GraphPad Prism 8.

### Treatment studies

Radiation studies were performed on athymic nude mice or BRG mice (C.Cg-*Rag2*$^{tm1Fwa}$ *Il2rg*$^{tm1Sug}$/JicTac; ref. 12). Mice were implanted with tumors in their right flank between 12 and 18 weeks of age. Established solid tumors were treated at 14–20 days later with BsAb and either Proteus[$^{225}$Ac] (37 kBq) or DOTA[$^{177}$Lu] (18.5–55.5 MBq).

### Anatomic and clinical pathology for toxicology assessment

Acute hematologic toxicities were assessed by automated complete blood count (CBC) Analysis (Drew Scientific) or Cytokine FLT3L ELISA (R&D Systems, catalog no., MFK00) according to the manufacturer's guidelines. Long-term toxicities were determined by complete necropsy and subsequent clinical or histologic analysis, with age-matched littermates for reference. Serum chemistry was evaluated on an AU 680 Chemistry Analyzer (Beckman Coulter Inc), see Supplementary Tables S6 and S7 for a complete list of analytes. Hematology was measured by automated CBC Analysis (Idexx Laboratories Inc.) and validated by manual differential. Tissues were fixed in formalin and embedded in paraffin blocks, sectioned at 5 μm, stained with hematoxylin and eosin (H&E), and examined by board-certified veterinary pathologists (See Supplementary Data for a complete list of tissues).

### Statistical analyses

All statistical analyses were performed using GraphPad Prism version 8.4. Statistical significances were determined by Mann–Whitney tests (ADA titers), two-way ANOVA with subsequent Sidak correction (tumor responses), or a log-rank Mantel–Cox test (survival analyses). For all statistical tests, a $P < 0.05$ was used to denote statistical significance.

## Results

### P53-SADA-BsAbs form stable tetramers with improved binding avidity

Previous reports have demonstrated that the optimal size for tumor penetrating proteins is between 150 and 200 kDa (13), while the renal clearance threshold has been estimated to be approximately 70 kDa (14). On the basis of this range, we designed a novel platform that fused small tetramerizing SADA domains to a humanized tandem single-chain fragment (scFv) BsAb: one scFv against ganglioside GD2 (15) and one scFv against radiometal-bearing DOTA (16). Candidate SADA domains were selected on the basis of several criteria, from the human proteome, soluble (nonmembrane), naturally tetramerizing, and small (<15 kDa), to create SADA–BsAbs that would be approximately 200 kDa when self-assembled and approximately 50 kDa when disassembled (**Fig. 1B**). Among the candidates identified (Supplementary Tables S1 and S2), P53-SADA-BsAb was deemed the most promising for clinical development. Binding studies using surface plasmon resonance (GE Healthcare, Biacore) confirmed P53-SADA-BsAb bound GD2 multivalently (**Fig. 2A**), displaying a slower dissociation rate and increased apparent binding affinity ($K_D$ = 1.2 nmol/L) compared with the corresponding anti-GD2 IgG-[L]-scFv formatted BsAb (IgG-scFv-BsAb, $K_D$ = 4.6 nmol/L; ref. 8).

### P53-SADA-BsAbs rapidly clear from the body without compromising tumor uptake

Serum pharmacokinetics analysis was performed on tumor-free NSG mice and demonstrated a 9-hour terminal half-life for P53-SADA-BsAb, with complete clearance from the blood within 48 hours (Supplementary Table S3). Notably, this was substantially slower than monomeric and dimeric anti-GD2 tandem-scFv BsAb ($t_{1/2}$ = 0.5 hour; ref. 17), while also faster and more complete than anti-GD2 IgG or IgG-scFv-BsAb ($t_{1/2}$ = 72 hours; ref. 10). Tumor uptake was measured

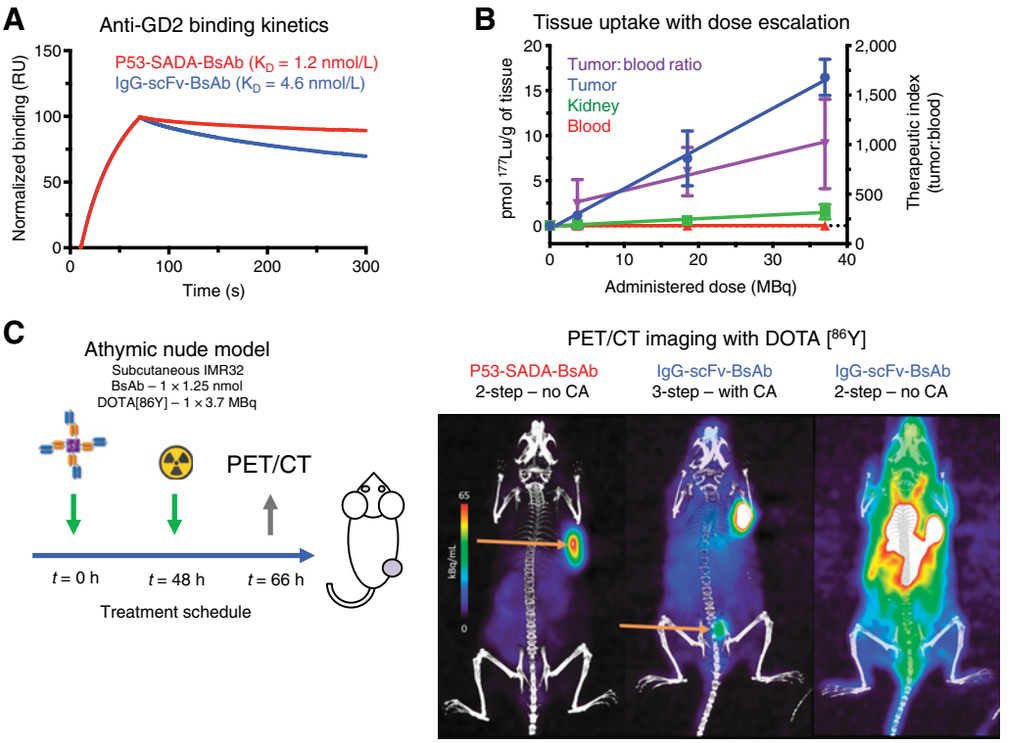


**Figure 2.**

*In vivo* pharmacokinetics and biodistribution of P53-SADA-BsAb. **A,** Normalized GD2 binding kinetics of P53-SADA-BsAb compared with IgG-scFv-BsAb, as measured by surface plasmon resonance. For each curve, maximum binding was normalized to 100. **B,** Relationship between administered dose and tissue uptake using two-step SADA-PRIT. Mice ($n = 5$ per group) were administered P53-SADA-BsAb (1.25 nmol) and one of three doses of DOTA[$^{177}$Lu]: 3.7, 18.5, or 37 MBq (20, 100, or 200 pmol, respectively). Blue represents level of DOTA payload in the tumor, green represents in the kidney, and red represents in the blood. The purple points represent the therapeutic index between tumor and blood at each dose. Tissue uptake was normalized to pmol of DOTA[$^{177}$Lu] per gram of tissue. **C,** PET/CT using P53-SADA-BsAb. Representative schematic (left) and images (right). Mice ($n = 1$–2) were injected with P53-SADA-BsAb or IgG-scFv-BsAb [with and without clearing agents (CA)] followed by DOTA[$^{86}$Y] (green lines correspond to each injection). Mice were imaged for 30 minutes (gray arrow) 18 hours after the administration of DOTA. Representative images are normalized using the same scale. Orange arrows point to the subcutaneous tumor (left) or the bladder (middle).

using two-step SADA-PRIT in athymic nude mice xenografts. Mice were dosed with P53-SADA-BsAb (1.25 nmol) and either 3.7, 18.5, or 37 MBq of DOTA[$^{177}$Lu] (20, 100, or 200 pmol, respectively). Tumor uptake revealed a strong linear correlation with administered dose (slope of 0.45 pmol/g/MBq; $R^2 = 0.94$), while activity in the blood remained low at all dose levels (slope < 0.001; $R^2 = 0.70$), resulting in higher tumor to blood ratios with higher doses of payload (**Fig. 2B**; Pearson coefficient of 0.9939). Kidney uptake also increased with administered dose, but with a much shallower slope (slope = 0.04; $R^2 = 0.77$). In contrast to previous studies of three-step IgG-PRIT (2), where tumor uptake plateaued at about 11 pmol/g, these results suggest that P53-SADA-BsAb may be able to more effectively deliver DOTA payloads to the tumor.

Dosimetry estimates for two-step SADA-PRIT were generated through serial biodistributions using the same animal model (Supplementary Table S4). On the basis of these findings, P53-SADA-BsAb was estimated to safely deliver an absorbed dose of 5,000 cGy to the tumor using a 15 MBq dose of DOTA[$^{177}$Lu] payload, with the kidneys and blood receiving only 191 and 44 cGy, respectively. On the basis of the linear dose–uptake relationship described above, further optimization should allow for continued improvements in these therapeutic indices.

To demonstrate the theranostic potential of P53-SADA-BsAb, we imaged mice using PET (**Fig. 2C**). Tumor-bearing athymic nude mice were dosed with P53-SADA-BsAb at $t = 0$ hour, followed by DOTA[$^{86}$Y] at $t = 48$ hours, and imaged at $t = 66$ hours (Supplementary Videos S1–S3). To accurately quantitate tissue uptake, mice were sacrificed, dissected, and counted directly after imaging (Supplementary Table S5). For comparison, two additional groups were included: mice dosed with (i) IgG-scFv-BsAb and DOTA[$^{86}$Y] without clearing agent (two-step) or (ii) IgG-scFv-BsAb and DOTA[$^{86}$Y] with clearing agent (three-step). As expected, two-step IgG-scFv-BsAb (no clearing agent) demonstrated significant retention of DOTA[$^{86}$Y] payload in the blood, while three-step IgG-scFv-BsAb (with clearing agent) improved tumor contrast, but also increased gut uptake. However, two-step P53-SADA-BsAb (without clearing agent) displayed the best contrast, with strong tumor uptake (31 %ID/g) and almost no detectable signal in any other organ (0.1 %ID/g in blood, 0.8 %ID/g in liver, and 0.3–0.8 %ID/g in gut).

## P53-SADA-BsAbs are much less immunogenic than IgG-scFv-BsAbs

Given their rapid clearance, we hypothesized P53-SADA-BsAbs may be less immunogenic than IgG-based therapies by avoiding the development of ADA. Such a benefit would be critical to clinical translation, where multiple doses of antibody might be needed. To test this hypothesis, we immunized (day 0) and challenged (day 28) immunocompetent tumor-free mice with P53-SADA-BsAb or

IgG-scFv-BsAb, and measured ADA titers in the plasma (Supplementary Fig. S1). Despite their high sequence homology, mice immunized with P53-SADA-BsAb showed significantly lower ADA titers than mice immunized with IgG-scFv-BsAb after both primary and secondary immunizations ($P = 0.008$).

### P53-SADA-BsAb safely delivers beta-emitter payloads to ablate established neuroblastoma tumors

The antitumor function of two-step SADA-PRIT was evaluated using a conventional 3 × 3 schedule, where each week for 3 weeks, tumor-bearing athymic nude mice received one dose of BsAb (1.25 nmol) followed by one dose of DOTA[$^{177}$Lu] (18.5 MBq, 100 pmol) 48 hours later (**Fig. 3A**). Within 2 weeks all treated tumors had decreased in size, and within 5 weeks they had completely responded (**Fig. 3B**), significantly extending survival (**Fig. 3C**, median survival >115 vs. 20 days for control groups; $P < 0.0001$). After up to 8 months of follow-up, 70% (7/10) of P53-SADA-BsAb–treated mice remained in complete remission.

Treatment-related toxicities stemming from P53-SADA-BsAb were determined after both short-term (0–30 days) and long-term (3–8 months) follow-up (Supplementary Fig. S2; Supplementary Table S6) and compared with three-step IgG-PRIT using the corresponding IgG-scFv-BsAb (8). Overall, toxicities were mild or absent in P53-SADA-BsAb–treated mice, there was no reduction in body weight, CBCs, plasma levels of cytokine FLT3L (a marker of bone marrow damage in mice and humans; refs. 18, 19), and serum chemistries were all normal, and histologic analyses of the bone marrow, liver, kidney, spleen, brain, and spine revealed no treatment-related pathologies. However, two treatment-related toxicities were observed. One mouse treated with P53-SADA-BsAb (of 9 checked) displayed mild to moderate ovarian atrophy (Supplementary Fig. S2), however, this was substantially less common and less severe than the ovarian toxicity observed in three-step IgG-PRIT (7/9 mice). In addition, one mouse (of 9 checked) displayed chronic cystitis of the bladder (Supplementary Fig. S2), an observation also made in the three-step IgG-PRIT–treated mice (1/9 mice), suggesting that the toxicity stemmed from DOTA[$^{177}$Lu] itself (which clears into the urine) and not the P53-SADA-BsAb.

### Two-step SADA-PRIT ablates established neuroblastoma PDX tumors using $^{177}$Lu

On the basis of the improved tumor dosimetry with larger doses of DOTA[$^{177}$Lu], we evaluated the impact of delivering a 3-fold more DOTA[$^{177}$Lu] per dose (55.5 MBq/dose, 300 pmol) using BRG mice bearing neuroblastoma PDXs (**Fig. 4A**). All treated mice demonstrated complete and durable responses (5/5 mice), while control groups had to be euthanized within 30 days due to tumor burden (**Fig. 4B** and **C**).

Consistent with the previous model, P53-SADA-BsAb–treated mice did not display any toxicity to the bone marrow, liver, kidney,

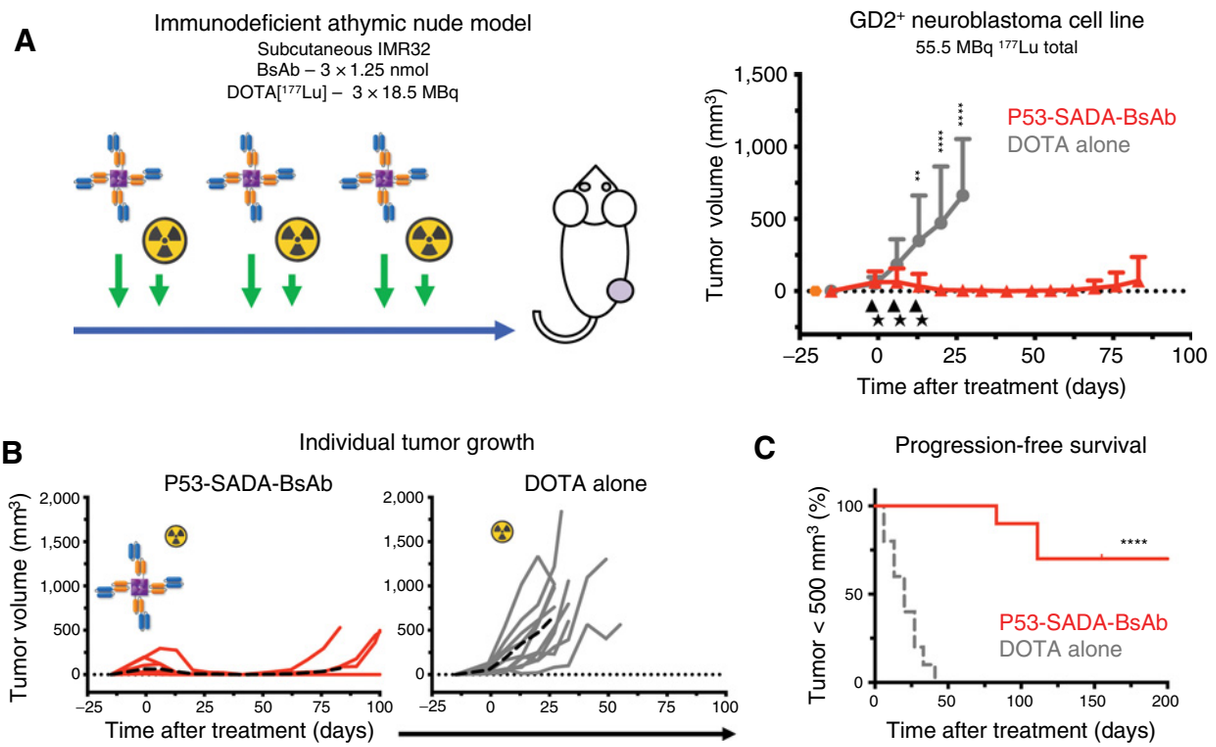


**Figure 3.**

Neuroblastoma xenograft treatment study. **A,** Schematic of treatment model (left) and mean tumor responses (right). Each dose of BsAb (1.25 nmol, triangle) was followed by one dose of DOTA[$^{177}$Lu] (18.5 MBq, star) 48 hours later. Each solid line represents one treatment group ($n = 10$). The black dotted line represents no measurable tumor, and the orange hexagon represents the tumor implantation. Tumor averages were calculated until at least one mouse had to be euthanized. **B,** Individual tumor responses. Each solid line represents tumors from a single mouse, and the dashed line represents the group average. **C,** Progression-free survival analysis. Each mouse was measured for tumor growth until tumors grew above 500 mm$^3$ in size. Mice were also censored for clinical pathology. No mice died unexpectedly. **, $P < 0.01$; ****, $P < 0.0001$ using two-way ANOVA (with Sidak correction) or log-rank (Mantel–Cox) test.

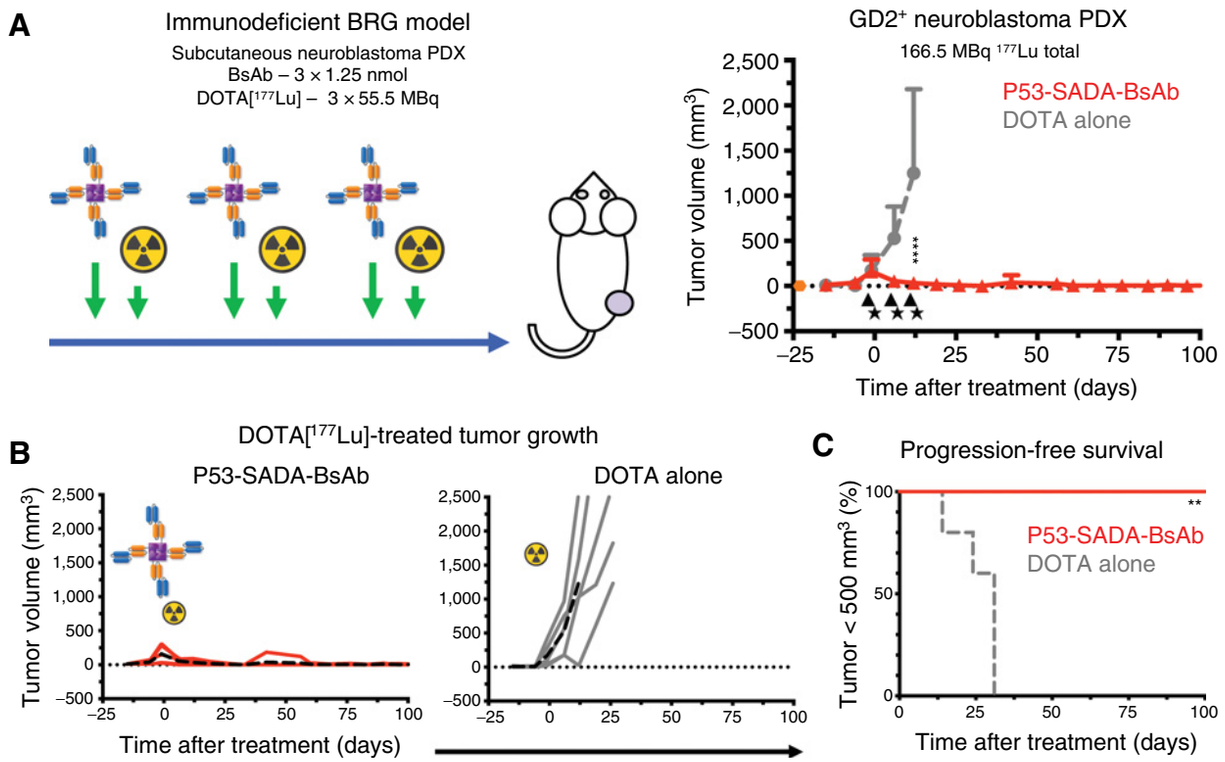


**Figure 4.**

Neuroblastoma PDX treated with DOTA[$^{177}$Lu]. **A,** Schematic of DOTA[$^{177}$Lu] treatment model (left) and mean tumor responses (right). Each dose of BsAb (1.25 nmol, triangle) was followed by one dose of DOTA[$^{177}$Lu] (55.5 MBq, star) 48 hours later. Each solid line represents one treatment group ($n = 5$). The black dotted line represents no measurable tumor, and the orange hexagon represents the tumor implantation. Tumor averages were calculated until at least one mouse had to be euthanized. **B,** Individual tumor responses. Each solid line represents tumors from a single mouse, and the dashed line represents the group average. **C,** Progression-free survival analysis. Each mouse was measured for tumor growth until tumors grew above 500 mm$^3$ in size. No mice died unexpectedly. **, $P < 0.01$; ****, $P < 0.0001$ using two-way ANOVA (with Sidak correction) or log-rank (Mantel–Cox) test.

spleen, brain, or spine (Supplementary Fig. S3; Supplementary Table S7), however, mice did display a more severe cystitis of the bladder. Because these mice received 3-fold more radioisotope than the previous model (**Fig. 2B**), the increased frequency and severity of the toxicity suggested that this amount of activity (6,600 MBq/kg $^{177}$Lu) was approaching the maximum tolerated dose (MTD) of the bladder. Notably, serum chemistries for all treated mice were normal at the time of sacrifice, and the mice did not show any signs of overt urinary dysfunction during or after treatment, indicating that this toxicity likely developed slowly over many weeks.

### Two-step SADA-PRIT ablates established neuroblastoma PDX tumors using $^{225}$Ac

We recently developed a novel chelator (Proteus) for delivering $^{225}$Ac (9), which uses a nonradioactive DOTA[$^{175}$Lu] handle for recognition by our anti-DOTA antibody, and sought to evaluate it using two-step SADA-PRIT. Here, BRG mice bearing the same neuroblastoma PDX tumors were treated with only one cycle of P53-SADA-BsAb (1.25 nmol) and Proteus[$^{225}$Ac] (37 kBq, 2.4 nmol; **Fig. 5A**). All mice treated with P53-SADA-BsAb and Proteus[$^{225}$Ac] responded, including one mouse which had a tumor more than 500 mm$^3$ in size (**Fig. 5A–C**), but no toxicities were observed (Supplementary Fig. S4; Supplementary Table S7). CBC analysis confirmed no acute myelosuppression and serum chemistry values remained normal 120 days after treatment. In addition, histologic examinations of all tissues revealed no evidence of radiation damage. Notably, bladder toxicity was entirely absent, confirming that the cystitis observed previously (Supplementary Fig. S3) came from the specific radioisotope used ($^{177}$Lu, perhaps due to its longer path length) and not the P53-SADA-BsAb itself. Many previous studies using $^{225}$Ac have been limited by renal toxicity (20–22), and because SADA-BsAb cleared primarily by renal filtration, kidneys from treated mice were more thoroughly analyzed for histologic changes. No treatment-related pathologies were observed by either H&E staining, terminal deoxynucleotidyl transferase–mediated dUTP nick end labeling staining, or cleaved caspase-3 IHC, confirming that two-step SADA-PRIT completely spared the kidneys.

### P53-SADA-BsAb can ablate established SCLC PDX tumors

Ganglioside GD2 is expressed in a broad spectrum of human tumors besides neuroblastoma (23). Among them, SCLC is perhaps the most difficult to treat (5-year survival <5%; ref. 24) and is currently undergoing clinical testing with an anti-GD2 IgG (NCT03098030). To evaluate its response to PRIT, we treated SCLC PDX–bearing (25) BRG mice (**Fig. 6**) with a single cycle of P53-SADA-BsAb (1.25 nmol) and Proteus[$^{225}$Ac] (37.5 kBq, 700 pmol). Despite their massive size at the time of treatment, all treated tumors responded. In addition, all, but one tumor, the largest among them, shrank completely and durably,

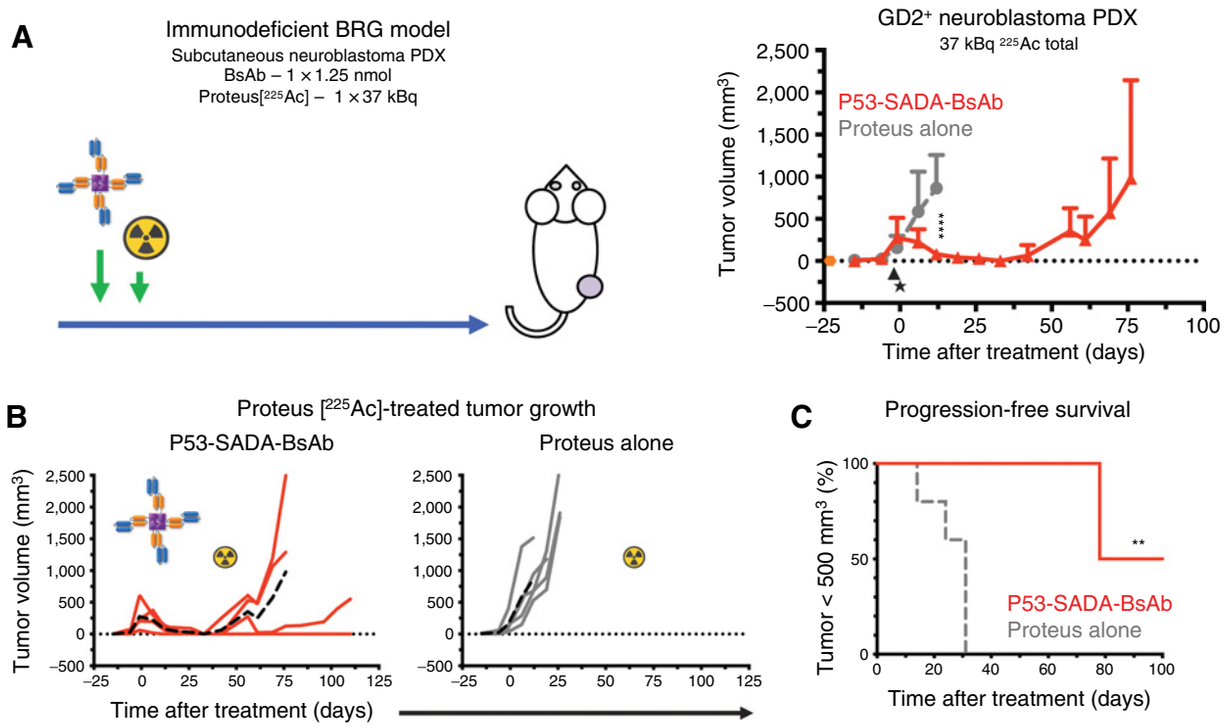


**Figure 5.**

Neuroblastoma PDX treated with Proteus[$^{225}$Ac]. **A,** Schematic of Proteus[$^{225}$Ac] treatment model (left) and mean tumor responses (right). Each dose of BsAb (1.25 nmol, triangle) was followed by one dose of Proteus[$^{225}$Ac] (37 kBq, star) 48 hours later. Each solid line represents one treatment group ($n = 5$). The black dotted line represents no measurable tumor, and the orange hexagon represents the tumor implantation. Tumor averages were calculated until at least one mouse had to be euthanized. **B,** Individual tumor responses. Each solid line represents tumors from a single mouse, and the dashed line represents the group average. **C,** Progression-free survival analysis. Each mouse was measured for tumor growth until tumors grew above 500 mm$^3$ in size. No mice died unexpectedly. **, $P < 0.01$; ****, $P < 0.0001$ using two-way ANOVA (with Sidak correction) or log-rank (Mantel–Cox) test.

while tumors in control groups rapidly grew out to the maximum allowed sizes.

## Discussion

In this study, we demonstrated that SADA domains can alter the pharmacokinetics of antibodies and sharply improve their therapeutic indices, a major hurdle for antibody- or peptide-targeted therapies. While many protein therapies benefit from long terminal half-lives (26), the delivery of highly cytotoxic payloads is inevitably dose limited by such platforms (27) and consequently this reduces antitumor efficacy. However, rapidly clearing peptides are not the solution either, because of their reduced bioavailability, poor tumor uptake, and high kidney retention (28). The SADA platform takes advantage of the narrow pharmacokinetics window between these two approaches, allowing for a plasma half-life just long enough to reach the tumor, and just short enough to be completely removed from the blood before payload administration. Furthermore, achieving this pharmacokinetics window resulted in substantially reduced immunogenicity, an important consideration for any therapeutic strategies that require multiple treatment cycles.

Previous attempts with multimerized delivery platforms have failed to achieve the desired therapeutic index because they lacked critical attributes unique to our design: (i) the use of human domains (P53) that avoided the immunogenicity or kidney retention problems seen with streptavidin (29); (ii) the monomer size (55 kDa) that allowed both the full tetramer (220 kDa) and dimer intermediates (110 kDa) to exceed the renal threshold, in contrast to previous studies where smaller monomers (30 kDa) resulted in dimers (60 kDa) that fell below renal filtration threshold (30); and (iii) the use of a DOTA payload that has minimal nonspecific uptake (31), in contrast to more hydrophobic haptens or peptides that are retained in the kidneys or other tissues (32).

Although treatment with P53-SADA-BsAb did not cause damage to any of the commonly radiosensitive tissues (bone marrow, liver, kidneys, and spleen; refs. 33–35), or natively GD2-expressing tissues (brain and spine; ref. 36), two notable toxicities were observed in this study. Cystitis of the bladder in mice treated with DOTA[$^{177}$Lu] appeared to be dose dependent and related to the transit of $^{177}$Lu through the bladder, but not P53-SADA-BsAb itself (no toxicity was observed with $^{225}$Ac). Thus, it is conceivable that any bladder damage could be minimized or even prevented with continuous emptying of the bladder (e.g., catherization and diuresis), or radioprotectants. In addition, some ovarian toxicity was observed, although substantially less often and less severely than among mice treated with conventional radioimmunotherapy or three-step IgG-PRIT (33). Both toxicities were observed in tissues not routinely examined during preclinical studies, making it difficult to know how common they may be in other approaches. Future studies, especially when using radiation, should, therefore, include complete histologic analyses to uncover these unanticipated toxicities before they reach patients, especially for pediatric indications.

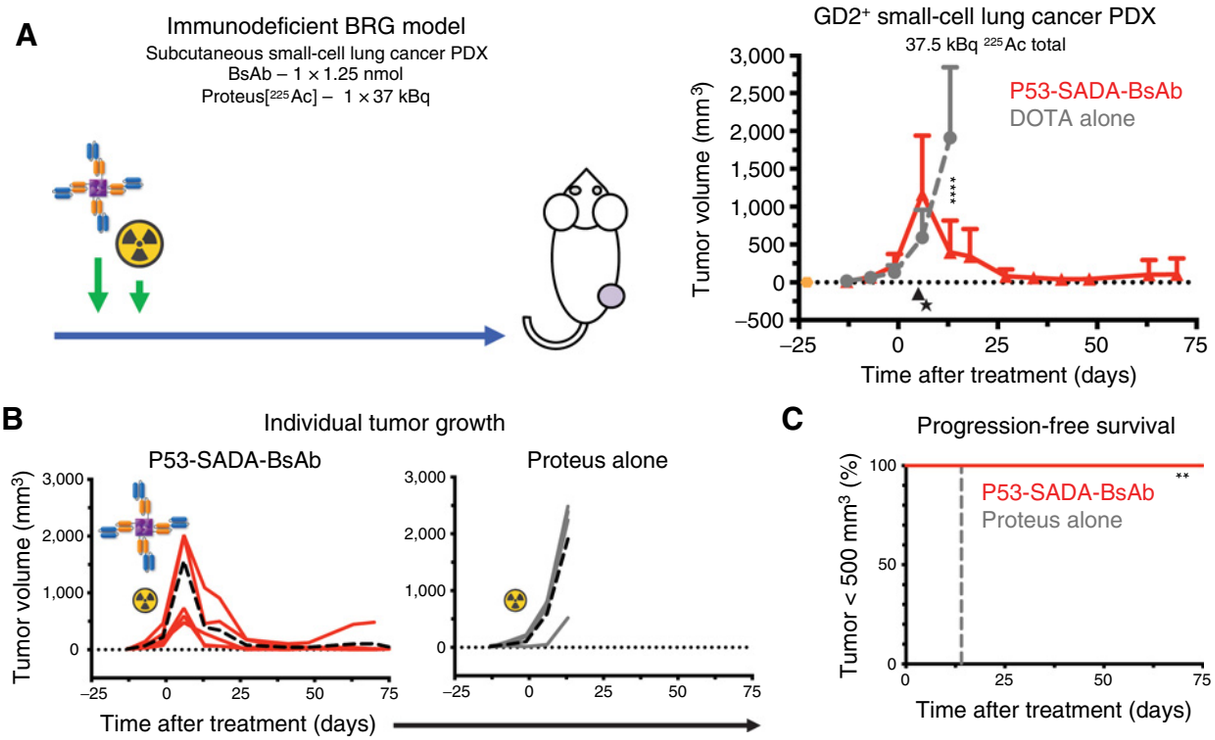


**Figure 6.**

SCLC PDX treatment study. **A,** Schematic of Proteus[$^{225}$Ac] treatment model (left) and mean tumor responses (right). One dose of BsAb (1.25 nmol, triangle) was followed by one dose of Proteus[$^{225}$Ac] (37 kBq, star) 48 hours later. Each line represents one treatment group ($n = 5$). The black dotted line represents no measurable tumor, and the orange hexagon represents the tumor implantation. Tumor averages were calculated until at least one mouse had to be euthanized. **B,** Individual tumor responses. Each solid line represents tumors from a single mouse, and the dashed line represents the group average. **C,** Progression-free survival analysis. Each mouse was measured for tumor growth until tumors grew above 500 mm$^3$ in size. No mice died unexpectedly. **, $P < 0.01$; ****, $P < 0.0001$ using two-way ANOVA (with Sidak correction) or log-rank (Mantel–Cox) test.

In conclusion, SADA has proven itself as a robust platform for the safe and effective targeted delivery of radioisotopes. It was efficacious without the need for clearing agent, and successfully treated two different aggressive solid tumors, neuroblastoma and SCLC. Given the striking lack of toxicity in the bone marrow, kidneys, or liver, SADA could provide substantial improvements in therapeutic index with other tumor targets or payloads, dramatically increasing antitumor efficacy while eliminating acute or long-term toxicities.

## Authors' Disclosures

B. H. Santich reports grants from Jeff Gordon Children's Foundation outside the submitted work and is listed as a coinventor on multiple patents regarding uses of the SADA technology to treat cancer, including uses that employ DOTA-isotope, compositions or methods using DOTA-isotopes (a fluorescent DOTA, methods of tracking immune cells with DOTA-isotopes), and specific antibody sequences for novel tumor antigens T-cell bispecific antibodies, all of which are owned by MSKCC and the first of which has been licensed to Y-mAbs Therapeutics. S.M. Cheal reports grants from NIH (R01 CA233896 and P30 CA008748) during the conduct of the study and is listed as a coinventor of a patent regarding Proteus[225Ac] owned by Memorial Sloan Kettering Cancer Center and licensed to Y-mAbs Therapeutics. M. Ahmed reports grants from Y-mAbs Therapeutics during the conduct of the study and is listed as a coinventor on a patent regarding SADA technologies owned by Memorial Sloan Kettering and licensed to Y-mAbs Therapeutics. M.R. McDevitt is listed as a coinventor on a patent regarding methods of radiolabeling antibodies with Ac225 owned by Memorial Sloan Kettering Cancer Center and licensed to another entity. O. Ouerfelli reports grants from NCI during the conduct of the study, other from Memorial Sloan Kettering Cancer Center during the conduct of the study and Memorial Sloan Kettering Cancer Center (intellectual property filed) outside the submitted work, and is listed as a coinventor on numerous patents unrelated to the submitted work, most related to prostate cancer drugs, owned by Memorial Sloan Kettering Cancer Center and licensed to Johnson & Johnson, Jazz Pharma, Y-mAbs Therapeutics, and AngioGenex, although some are not licensed. G. Yang reports other from Memorial Sloan Kettering Cancer Center (intellectual property), Y-mAbs Therapeutics (intellectual property) and Memorial Sloan Kettering Cancer Centre (intellectual property) outside the submitted work, and personal fees from JNJ during the conduct of the study, and is listed as a coinventor on a patent regarding N-Acetylgalactosamino dendron-clearing agent for DOTA-pretargeted radioimmunotherapy owned by Memorial Sloan Kettering Cancer Center and licensed to Y-mAbs Therapeutics. E.K. Fung reports personal fees from Y-mAbs Therapeutics outside the submitted work. C.M. Rudin reports personal fees from AbbVie, Amgen, AstraZeneca, Bicycle, Celgene, Genentech/Roche, Ipsen, Janssen, Jazz, PharmaMar, Pfizer, Syros, Vivotek, Harpoon Therapeutics (SAB), and Bridge Medicines (SAB) outside the submitted work. S.M. Larson reports grants and other from Y-mAbs Therapeutics (stock), other from Elucida Therapeutics (founders stock) and Imaging Inc. (scientific advisory board), and is listed as a coinventor on a patent regarding radiohapten capture by bifunctional proteins owned by Y-mAbs Therapeutics. N.K. Cheung reports grants from Isabella Santos Foundation and Jeff Gordon Children's Foundation during the conduct of the study, grants and personal fees from Y-mAbs Therapeutics and Abpro Labs, personal fees from Eureka Therapeutics, and is listed as a coinventor on a patent regarding modular self-assembly disassembly (SADA) technologies owned by Memorial Sloan Kettering and licensed to Y-mAbs Therapeutics. No disclosures were reported by the other authors.

## Authors' Contributions

**B.H. Santich:** Conceptualization, data curation, formal analysis, validation, investigation, methodology, writing-original draft, project administration, writing-review and editing. **S.M. Cheal:** Resources, formal analysis, validation, investigation, methodology, project administration. **M. Ahmed:** Conceptualization, investigation,

writing-review and editing. **M.R. McDevitt:** Resources, methodology. **O. Ouerfelli:** Resources. **G. Yang:** Resources. **D.R. Veach:** Resources, methodology. **E.K. Fung:** Formal analysis, visualization, methodology. **M. Patel:** Methodology. **D. Burnes Vargas:** Methodology. **A.A. Malik:** Formal analysis, methodology. **H.-F. Guo:** Resources, methodology. **P.B. Zanzonico:** Resources, formal analysis, methodology. **S. Monette:** Formal analysis, methodology, writing-review and editing. **A.O. Michel:** Formal analysis, methodology. **C.M. Rudin:** Resources, formal analysis, investigation, writing-review and editing. **S.M. Larson:** Resources, formal analysis, investigation, methodology, writing-review and editing. **N.K. Cheung:** Conceptualization, supervision, funding acquisition, investigation, project administration, writing-review and editing.

## Acknowledgments

We thank Dr. Elisa de Stanchina for her help in developing and passaging the patient-derived xenograft tumors. We also thank Rebecca Wilen for help with protein expression. This work was supported by funds from the Isabella Santos Foundation (to N.K. Cheung), the Jeff Gordon Children's Foundation (to N.K. Cheung), Enid A. Haupt Endowed Chair (to N.K. Cheung), the Robert Steel Foundation (to N.K. Cheung), the Grayer Fellowship (to B.H. Santich), Experimental Therapeutics Center of MSKCC (to S.M. Larson), R01 CA233896 (to S.M. Cheal), the MSKCC Core Grants (P30 CA008748), and a sponsored research agreement from Y-mAbs Therapeutics.

The costs of publication of this article were defrayed in part by the payment of page charges. This article must therefore be hereby marked *advertisement* in accordance with 18 U.S.C. Section 1734 solely to indicate this fact.

Received June 2, 2020; revised July 22, 2020; accepted September 15, 2020; published first September 21, 2020.

## References

1. Chaffer CL, Weinberg RA. A perspective on cancer cell metastasis. Science 2011;331:1559–64.
2. Cheal SM, Xu H, Guo HF, Lee SG, Punzalan B, Chalasani S, et al. Theranostic pretargeted radioimmunotherapy of colorectal cancer xenografts in mice using picomolar affinity $^{86}$Y- or $^{177}$Lu-DOTA-Bn binding scFv C825/GPA33 IgG bispecific immunoconjugates. Eur J Nucl Med Mol Imaging 2016;43:925–37.
3. Lin A, Giuliano CJ, Palladino A, John KM, Abramowicz C, Yuan ML, et al. Off-target toxicity is a common mechanism of action of cancer drugs undergoing clinical trials. Sci Transl Med 2019;11:eaaw8412.
4. Coats S, Williams M, Kebble B, Dixit R, Tseng L, Yao N-S, et al. Antibody–drug conjugates: future directions in clinical and translational strategies to improve the therapeutic index. Clin Cancer Res 2019;25:5441–8.
5. Larson SM, Carrasquillo JA, Cheung NK, Press OW. Radioimmunotherapy of human tumours. Nat Rev Cancer 2015;15:347–60.
6. Houghton JL, Membreno R, Abdel-Atti D, Cunanan KM, Carlin S, Scholz WW, et al. Establishment of the *in vivo* efficacy of pretargeted radioimmunotherapy utilizing inverse electron demand Diels-Alder click chemistry. Mol Cancer Ther 2017;16:124–33.
7. Cheal SM, Patel M, Yang G, Veach DR, Xu H, Guo HF, et al. A N-acetylgalactosamino dendron-clearing agent for high-therapeutic index DOTA-hapten pretargeted radioimmunotherapy. Bioconjug Chem 2020;31:501–6.
8. Cheal SM, Xu H, Guo HF, Zanzonico PB, Larson SM, Cheung NK. Preclinical evaluation of multistep targeting of diasialoganglioside GD2 using an IgG-scFv bispecific antibody with high affinity for GD2 and DOTA metal complex. Mol Cancer Ther 2014;13:1803–12.
9. Cheal SM, McDevitt MR, Santich BH, Patel M, Yang G, Fung EK, et al. Alpha radioimmunotherapy using 225Ac-proteus-DOTA for solid tumors – safety at curative doses. Theranostics 2020. DOI: 10.7150/thno.48810.
10. Santich BH, Park JA, Tran H, Guo HF, Huse M, Cheung NV. Interdomain spacing and spatial configuration drive the potency of IgG-[L]-scFv T cell bispecific antibodies. Sci Transl Med 2020;12:eaax1315.
11. Cheng M, Santich BH, Xu H, Ahmed M, Huse M, Cheung NK. Successful engineering of a highly potent single-chain variable-fragment (scFv) bispecific antibody to target disialoganglioside (GD2) positive tumors. Oncoimmunology 2016;5:e1168557.
12. Xu H, Cheng M, Guo H, Chen Y, Huse M, Cheung NK. Retargeting T cells to GD2 pentasaccharide on human tumors using bispecific humanized antibody. Cancer Immunol Res 2015;3:266–77.
13. Schmidt MM, Wittrup KD. A modeling analysis of the effects of molecular size and binding affinity on tumor targeting. Mol Cancer Ther 2009;8:2861–71.
14. Knauf MJ, Bell DP, Hirtzer P, Luo ZP, Young JD, Katre NV. Relationship of effective molecular size to systemic clearance in rats of recombinant interleukin-2 chemically modified with water-soluble polymers. J Biol Chem 1988;263:15064–70.
15. Cheung NK, Guo H, Hu J, Tassev DV, Cheung IY. Humanizing murine IgG3 anti-GD2 antibody m3F8 substantially improves antibody-dependent cell-mediated cytotoxicity while retaining targeting *in vivo*. Oncoimmunology 2012;1:477–86.
16. Orcutt KD, Slusarczyk AL, Cieslewicz M, Ruiz-Yi B, Bhushan KR, Frangioni JV, et al. Engineering an antibody with picomolar affinity to DOTA chelates of multiple radionuclides for pretargeted radioimmunotherapy and imaging. Nucl Med Biol 2011;38:223–33.
17. Ahmed M, Cheng M, Cheung IY, Cheung NK. Human derived dimerization tag enhances tumor killing potency of a T-cell engaging bispecific antibody. Oncoimmunology 2015;4:e989776.
18. Siegel JA, Yeldell D, Goldenberg DM, Stabin MG, Sparks RB, Sharkey RM, et al. Red marrow radiation dose adjustment using plasma FLT3-L cytokine levels: improved correlations between hematologic toxicity and bone marrow dose for radioimmunotherapy patients. J Nucl Med 2003;44:67–76.
19. Prat M, Demarquay C, Frick J, Thierry D, Gorin NC, Bertho JM. Radiation-induced increase in plasma Flt3 ligand concentration in mice: evidence for the implication of several cell types. Radiat Res 2005;163:408–17.
20. Jaggi JS, Seshan SV, McDevitt MR, LaPerle K, Sgouros G, Scheinberg DA. Renal tubulointerstitial changes after internal irradiation with alpha-particle-emitting actinium daughters. J Am Soc Nephrol 2005;16:2677–89.
21. Miederer M, McDevitt MR, Sgouros G, Kramer K, Cheung NK, Scheinberg DA. Pharmacokinetics, dosimetry, and toxicity of the targetable atomic generator, 225Ac-HuM195, in nonhuman primates. J Nucl Med 2004;45:129–37.
22. Poty S, Carter LM, Mandleywala K, Membreno R, Abdel-Atti D, Ragupathi A, et al. Leveraging bioorthogonal click chemistry to improve 225Ac-radioimmunotherapy of pancreatic ductal adenocarcinoma. Clin Cancer Res 2019;25:868–80.
23. Suzuki M, Cheung NK. Disialoganglioside GD2 as a therapeutic target for human diseases. Expert Opin Ther Targets 2015;19:349–62.
24. Oronsky B, Reid TR, Oronsky A, Carter CA. What's new in SCLC? A review. Neoplasia 2017;19:842–7.
25. Daniel VC, Marchionni L, Hierman JS, Rhodes JT, Devereux WL, Rudin CM, et al. A primary xenograft model of small-cell lung cancer reveals irreversible changes in gene expression imposed by culture *in vitro*. Cancer Res 2009;69:3364–73.
26. Bell SJ, Fam CM, Chlipala EA, Carlson SJ, Lee JI, Rosendahl MS, et al. Enhanced circulating half-life and antitumor activity of a site-specific pegylated interferon-α protein therapeutic. Bioconjugate Chem 2008;19:299–305.
27. Muselaers S, Boers-Sonderen M, Oostenbrugge Tv, Boerman O, Desar I, Stillebroer A, et al. Phase II study of lutetium-177-labeled anti-carbonic anhydrase IX monoclonal antibody girentuximab in patients with advanced renal cell carcinoma. J Nucl Med 2016;57:34.
28. Pavlinkova G, Beresford GW, Booth BJ, Batra SK, Colcher D. Pharmacokinetics and biodistribution of engineered single-chain antibody constructs of MAb CC49 in colon carcinoma xenografts. J Nucl Med 1999;40:1536–46.
29. Cheung NK, Modak S, Lin Y, Guo H, Zanzonico P, Chung J, et al. Single-chain Fv-streptavidin substantially improved therapeutic index in multistep targeting directed at disialoganglioside GD2. J Nucl Med 2004;45:867–77.
30. Kubetzko S, Balic E, Waibel R, Zangemeister-Wittke U, Pluckthun A. PEGylation and multimerization of the anti-p185HER-2 single chain Fv fragment 4D5: effects on tumor targeting. J Biol Chem 2006;281:35186–201.
31. Orcutt KD, Nasr KA, Whitehead DG, Frangioni JV, Wittrup KD. Biodistribution and clearance of small molecule hapten chelates for pretargeted radioimmunotherapy. Mol Imaging Biol 2011;13:215–21.
32. Goldenberg DM, Rossi EA, Sharkey RM, McBride WJ, Chang CH. Multifunctional antibodies by the dock-and-lock method for improved cancer imaging and therapy by pretargeting. J Nucl Med 2008;49:158–63.

33. Repetto-Llamazares AH, Larsen RH, Giusti AM, Riccardi E, Bruland OS, Selbo PK, et al. $^{177}$Lu-DOTA-HH1, a novel anti-CD37 radio-immunoconjugate: a study of toxicity in nude mice. PLoS One 2014;9:e103070.
34. Cheung NK, Landmeier B, Neely J, Nelson AD, Abramowsky C, Ellery S, et al. Complete tumor ablation with iodine 131-radiolabeled disialoganglioside GD2-specific monoclonal antibody against human neuroblastoma xenografted in nude mice. J Natl Cancer Inst 1986;77:739–45.
35. Subbiah K, Hamlin DK, Pagel JM, Wilbur DS, Meyer DL, Axworthy DB, et al. Comparison of immunoscintigraphy, efficacy, and toxicity of conventional and pretargeted radioimmunotherapy in CD20-expressing human lymphoma xenografts. J Nucl Med 2003;44:437–45.
36. Furukawa K, Aixinjueluo W, Kasama T, Ohkawa Y, Yoshihara M, Ohmi Y, et al. Disruption of GM2/GD2 synthase gene resulted in overt expression of 9-O-acetyl GD3 irrespective of Tis21. J Neurochem 2008;105:1057–66.